RESEARCH FRONT

CSIRO PUBLISHING

Environ. Chem.
http://dx.doi.org/10.1071/EN14072

Research Paper

A pilot interlaboratory comparison of protocols that simulate aging of nanocomposites and detect released fragments

Wendel Wohlleben,[A,E] *Gemma Vilar,*[B] *Elisabet Fernández-Rosas,*[B] *David González-Gálvez,*[B] *Claus Gabriel,*[C] *Sabine Hirth,*[A] *Thomas Frechen,*[A] *Deborah Stanley,*[D] *Justin Gorham,*[D] *Li-Piin Sung,*[D] *Hsiang-Chun Hsueh,*[D] *Yu-Fan Chuang,*[D] *Tinh Nguyen*[D,E] *and Socorro Vazquez-Campos*[B,E]

[A]BASF SE, Advanced Materials and Systems Research, Department of Material Physics, D-67056 Ludwigshafen, Germany.
[B]LEITAT Technological Center, c/de la Innovació 2, E-08225 Terrassa (Barcelona), Spain.
[C]BASF SE, Advanced Materials and Systems Research, Department of Structural Materials, D-67056 Ludwigshafen, Germany.
[D]National Institute of Standards and Technology, 100 Bureau Drive, Gaithersburg, MD 20899, USA.
[E]Corresponding authors. Email: wendel.wohlleben@basf.com; tinh.nguyen@nist.gov; svazquez@leitat.org

Environmental context. Nanoparticles are contained in many commercialised products, but the lack of validated methods to assess their potential release into the environment hampers our ability to perform a reliable risk assessment. Equipment to simulate aging is available, but the challenge is to sample released entities, and to analyse those fragments with suitable nano-analytics. We describe methods to characterise the degradation and surface accumulation of nanoparticles, and to quantify fragments released during UV irradiation of polymer nanocomposites.

Abstract. The safe use of nanoparticles as fillers in nanocomposite materials depends, in part, on a good understanding of what is released from aging nanocomposites, and at which rate. Here we investigated the critical parameters of the nanoparticle release phenomenon by a pilot inter-laboratory study of a polyamide containing 4 mass % of silica nanoparticles (nanosilica). The main focus is on the validity range of the aging and release protocols. Both induced release by mechanical shear after dry weathering at different UV intensities and spontaneous release during wet weathering were investigated. We propose a combined protocol based on the finding that the characteristics of released fragments – which are the essential input for fate, transport and (eco-)toxicological testing – were reproducible between laboratories and between different aging, sampling and analysis protocols: the released fragments were a polydisperse mixture of predominantly composite fragments from the nanometre up to several micrometre diameter, and of clustered or individual nanosilica unbound to polymer. The unbound fraction was microscopically observed but could not be quantified. We found that aging conditions are very critical for the release rates, not for release characteristics. The sampling protocol tolerates some differences. Simplified aging + immersion protocols can at least partially replace, complement and extend dedicated weathering apparatus with run-off collection.

Additional keywords: dry aging, lifecycle, nanosilica, polyamide, release, wet aging.

Received 5 April 2014, accepted 28 June 2014, published online 8 August 2014

Introduction

Nanofillers in the forms of particles, fibres or platelets are increasingly embedded in polymers (i.e. polymer nanocomposites) to enhance their performance. In order to complement and modify the properties of the polymer matrix, these fillers are often metal oxide, ceramic or carbon-based nanomaterials. Concern has been raised about the toxicokinetic properties on humans exposed to these nanomaterials and about the fate and effect of nanomaterials dispersed into the environment. The safety of nanocomposite materials hence depends on our understanding of the probability of release of nanofillers throughout the nanocomposite's lifecycle.[1–3] To simulate the year-long outdoor use by consumers, International Organization for Standardization (ISO)-standardised weathering tests are well established for plastics and coatings. Of note, these materials have always been nanocomposites owing to the sizes of the embedded pigments and fillers, so that the established weathering tests should be amenable to release testing if we devise valid protocols of release sampling and characterisation.[4] The photolysis and hydrolysis of polymer nanocomposites has been

linked primarily to the degradation behaviour of the polymer matrix, which can be modulated by the embedded nanomaterials such as SiO_2,[5–7] multiwalled-carbon nanotubes (MWCNTs)[5,8–12] or graphene.[13] The objective of the present interlaboratory comparison of weathering protocols is to identify critical elements of aging, sampling and detection methods, and to derive a recommendation for a unified protocol.

Polyamide (PA) materials have been chosen as a test case, because these polymers are used extensively for many outdoor applications. However, because of the presence of the low dissociation energy C–N bonds (53 kcal mol^{-1}) and the electron rich nitrogen atom in the main chain, this polymer is susceptible to attack by UV light at short (254 nm) and long (>295 nm) wavelengths.[14–16] Under a UV wavelength >295 nm, which is used in this study and present in the sun's spectrum at ground level, both direct photo-scission of the C–N bonds and photo-oxidation of PA occurs,[14,16] leading to chain scission and formation of various oxidised products, including hydroperoxides, aldehydes, imides (CO–NH–CO) and carboxylic acids. These authors also showed that the photo-oxidation of this polymer is strongly affected by the presence of water.[14,16] Photodegradation of the PA chemical structure leads to the loss of its performance, such as a decrease in mechanical property, yellowing and cracking.

The nanomaterial (NM) lifecycle perspective requires protocols that couple aging and weathering setups with methods to sample, identify, quantify and characterise the released fragments (released fragments include both polymer-embedded and polymer-free nanofillers). Proposed protocols include UV + rain weathering with the sampling of fragments from run-off waters,[7,17] UV irradiation followed by immersion,[18,19] UV irradiation followed by spraying[20] or UV irradiation followed by air streams or sanding.[21] Several of these protocols employ UV irradiation as specified by ISO 4892–2,[22] but none of the protocols has been replicated on the same nanocomposite exposed to the same or different weathering apparatus in different laboratories.

Here we explored the relation between spontaneous release and induced release,[4] and assessed the origin of variations in the results, by a pilot interlaboratory comparison to simulate aging and characterise the release of hydrophobised SiO_2 nanoparticles (nanosilica) from PA nanocomposites. We expected that the protocols employed for specimen aging and release sampling have profound influence on the characteristics of release and on release rates (quantities). Both induced release by mechanical shear *after* dry weathering at different UV intensities and spontaneous release *during* wet weathering were investigated using a variety of techniques to characterise the degradation and nanoparticle surface accumulation and to quantify release fragments during UV irradiation of polymer nanocomposites.

Materials and methods[A]

PA nanosilica composites

The PA matrix was a low viscosity general-purpose, extrusion PA6 grade material (BASF, Ludwigshafen, Germany) well suited for compounding. It conformed to FDA requirements including 21 CFR 177.1500, EU Directive2002/72/EC and the German BfR recommendation 'X Polyamide', 1.6.1998. The fumed powdered silica nanoparticles (nanosilica) of the grade Aerosil R8200 (Evonik, Essen, Germany) had primary diameters of 8 to 20 nm and were of approximately spherical shape with partial aggregation and a thin hexamethyldisilazane (siloxane) surface coating (Figs S1 to S4). The nanosilica at a nominally 4 mass % (g g^{-1}) was compounded into the PA at 280 °C by a ZSK 18 twin-screw extruder (Coperion, Stuttgart, Germany) at a rate of 2.8 kg h^{-1} and then pelletted. The 3-mm pelletts were dried at 70 °C for 1 week and then melt-pressed at 240 °C into round plates of 11-cm diameter and 1-mm thickness. These plates were distributed to all three laboratories: BASF (Ludwigshafen, Germany), LEITAT (Terrassa, Barcelona, Spain) and the National Institute of Standards and Technology (NIST) (Gaithersburg, MD, USA).

Fourier transform infrared (FTIR) spectra, thermogravimetric analysis (TGA) scans, X-ray photoelectron (XPS) spectra, and thin-cut transmission electron microscopy (TEM) images were obtained on as-produced (non-aged) samples from both neat PA and the PA–nanosilica composite, and the results are presented in the first section of the Supporting Information (Figs S1 to S4). The characteristic vibration bands, decomposition temperatures, photoelectron spectra and surface morphologies serve for identification of the composition of fragments after weathering.

The actual nanosilica content in the plates was confirmed by TGA (3.8 mass %, Table S1). The matching results (5 mass %) from the XPS technique that examined only the top 10 nm of the plate confirm that the silica nanoparticles are homogeneously distributed up to the surface. However, TEM analysis of microtome slices revealed that the filler dispersion in the nanocomposite was incomplete. The filler was present in the form of clusters up to 200 nm that may contain voids, which were absent in the unfilled PA reference. TGA of neat PA indicated the presence of 0.83 % silicon derivatives from impurities (Fig. S3).

The FTIR bands (Fig. S1) corresponded to amide polymers: the A band at 3292 cm^{-1} was attributed to –NH– stretching from the amide groups, at 2934 and 2864 cm^{-1} to the C^3_{sp}–H stretching, and at 1634 and 1537 cm^{-1} to carbonyl (C=O) stretching and –NH– bending respectively of the amide groups. The characteristic band peaking at 1060 cm^{-1} associated with the SiO_2 vibrations (–Si–O–Si stretching, Fig. S1) were observed in the PA–nanosilica composite sample (Fig S1).

UV exposures, sampling and characterisation at LEITAT, Spain

The neat PA and PA–nanosilica composite samples were submitted to ISO-standardised accelerated aging as specified in Table 1. Dose (MJ m^{-2}) was defined in this study as the total energy of UV radiation impinging on the sample surface at a particular time per unit irradiated area.

The position of the samples was changed every 250 h for homogeneous UV and rain exposure. Run-off waters were collected separately. The climate chamber was cleaned with extra water to assure that all released material was collected in run-off water containers. Four samples of 1 L of the run-off water were collected for each material as representative fractions. These samples were lyophilised by freeze drying (CoolSafe 100–9 PRO Freeze Dryer (LaboGene ApS; Lynge, Denmark),

[A]Certain commercial product or equipment is described in this paper in order to specify adequately the experimental procedure. In no case does such identification imply recommendation or endorsement by the National Institute of Standards and Technology, nor does it imply that it is necessarily the best available for the purpose.

Table 1. Protocols of aging, sampling and detection

SEM, scanning electron microscopy; XPS, X-ray photoelectron spectroscopy; AFM, atomic force microscopy; LCSM, laser scanning confocal microscopy; FTIR, Fourier-transform infrared spectroscopy; TEM, transmission electron microscopy; EDX, energy-dispersive X-ray spectroscopy; AUC-RI, analytical ultracentrifugation with refractive index detector; ICP-MS, inductively coupled plasma–mass spectrometry; TGA, thermogravimetric analysis

Laboratory	BASF	LEITAT	NIST
Wet aging equipment	CI 4000, Atlas	Suntest XXL+, Atlas	–
Dry aging equipment	Suntest XLS+, Atlas	–	SPHERE
Applicable Standard	ISO 4892-2 (2013)	ISO 4892-2 (2013)	–
UV source	Xenon, 60 W m^{-2} between 300 and 400 nm	Xenon, 60 W m^{-2} between 300 and 400 nm	Mercury, 140 W m^{-2} between 295 and 400 nm
Wet/dry cycles	18 min/102 min (ISO 4892-2 Table 3)	1 ± 0.5 min/29 min (NanoPolyTox protocol)	–
Temperature	65 °C at blackbody sensor	65 °C at blackbody sensor	65 °C at specimen
Specimen dimensions	11-cm diameter, 1-mm thickness	11-cm diameter, 1-mm thickness	2.5 × 2.5 cm, 1-mm thickness
UV doses for specimen aging characterisation	145–290–435 MJ m^{-2}	216 MJ m^{-2}	12–36–72–120–193–290–386–543–700–833 MJ m^{-2}
Characterisation of aged specimen surface	SEM, XPS	–	Mass loss, XPS, AFM, LCSM, FTIR
UV doses for release sampling	145–290–435 MJ m^{-2}	216 MJ m^{-2}	193–290–386–833 MJ m^{-2}
Release sampling method	Aged surface immersed in 3.5 mL of H_2O (0.5 g L^{-1} SDS), standing still for 24 h, 0.5 mL sampled and then shaken for 24 h, 5 Hz, 3 mm amplitude, 0.5 mL sampled and then sonication for 1 h, 0.5 mL sampled → simulate continued outdoor use	Collect run-off water during aging then lyophilise → simulate spontaneous environmental release. Additionally, immersion was performed at BASF using the same protocol (cf. left of this table)	Immersion was performed at BASF using the same protocol (cf. left of this table)
Detection and characterisation of released fragments	TEM, EDX, AUC-RI, ICP-MS	TEM, EDX, FTIR, TGA	–

water sublimation at −95 °C and ~0.3 mbar) in order to isolate the released materials. A blank was performed for every weathering process: 1 L of run-off water coming from an empty position was also lyophilised to assure no material was due to other processes in the chamber. Some of the material extracted was calcined (700 °C, 30 min) to isolate the nanosilica and better characterise it.

Collected materials were characterised by TGA, FTIR, TEM and energy-dispersive X-ray spectroscopy (EDX). Thermal degradation of released materials was studied by Hi-Res TGA (Q500; TA instruments, New Castle, DE, USA), using a temperature rate increase of 10 °C min^{-1} from 30 to 1000 °C and an air flow rate of 50 mL min^{-1}. Mass losses below 160 °C were not considered to avoid errors due to sample hydration during the aging process. A FTIR spectrophotometer (IR Affinity-1 8400, Shimadzu, Kyoto, Japan) was used to identify the different functional groups present in the released samples. Both transmission FTIR of 1 mass % analyte in 99 % KBr pellets and attenuated total reflectance (ATR) FTIR of an unexposed nanocomposite plate were performed. TEM (JEM 2011; JEOL Ltd, Akishima, Tokyo, Japan) equipped with a CCD camera (USC 4000, model 895; Gatan Inc., Pleasanton, CA, USA) and an EDX detector (EDS X-ManN 80T; Oxford Instruments plc, Abingdon, UK) was used for morphological analysis of the released materials and to determine their atomic composition. Samples were deposited on TEM grids (formvar/carbon-coated 200 mesh Cu grids, Ted Pella Inc., Redding, CA, USA) just after their dispersion in ultrapure water.

We expected that the aging and sampling using this protocol is the closest to that resulting in spontaneous release of nanocomposites in e.g. architectural outdoor applications, but it was uncertain to what extent the extreme dilution in run-off waters would hamper the ensuing analysis.

UV exposures and characterisation at BASF, Germany

Simulated weathering was performed by UV irradiation both under dry conditions and with rain-cycles as specified in Table 1, all adhering directly to ISO-standardised protocols.[22] As the wet aging was in a multipurpose apparatus with many different samples in parallel, the run-off waters from exposures in this apparatus were not recycled or collected, and they were discarded without analysis.

The scanning electron microscopy (SEM) measurements of degraded surfaces were performed with a JEOL JSM-7500 TFE SEM at an accelerating voltage of 5 kV. The sample surfaces were sputtered with an ~15 nm-thin Pt layer before SEM imaging in order to prevent charging of the surfaces due to the electron beam. Additionally, backscatter electron imaging was performed to highlight inorganic components.

We expected that this ISO-based protocol would be highly reproducible and easily transferrable between laboratories, with the main uncertainties linked to the immersion sampling of release as described below.

UV exposures and characterisation at NIST, USA

Samples of neat PA and the PA–nanosilica composite were irradiated with UV light for different doses as specified in Table 1 in the NIST 2-m integrating sphere-based weathering chamber, referred to as SPHERE (Simulated Photodegradation by High Energy Radiant Exposure).[23] The SPHERE UV chamber employed a mercury arc lamp system that generated a collimated and highly uniform UV radiation flux. Because the visible and IR radiation of the UV source for the SPHERE UV chamber had been removed, the temperature in the SPHERE was usually ~27 °C. An external heating source was employed to provide the 65 °C temperature used in this study. The relative humidity (RH) of the exposure chamber could be maintained to

within 2 % of the preset values, whereas the temperature can be controlled to ±0.5 °C. Samples mounted on special sample holders were removed at specified accumulated doses (e.g. at specified time intervals) for characterisation. Mass loss, surface morphology and chemical degradation of neat PA and the PA–nanosilica composite as a function of UV dose in the NIST SPHERE were characterised. The mass loss was determined using an analytical balance having a mass resolution of 10^{-5} g (Mettler Toledo AB265-S). Mass loss results were the average of four specimens. Surface morphological changes were characterised by tapping mode AFM and laser scanning confocal microscopy (LSCM). AFM imaging was carried out at ambient conditions (24 °C, 50 % RH) using a Dimension 3100 system (Veeco Metrology, Santa Barbara, CA, USA) and silicon probes (TESP 70, Veeco Metrology). Both topographic (height) and phase images were obtained simultaneously using a resonance frequency of 300 kHz for the probe oscillation and a free-oscillation amplitude of 62 ± 2 nm. The phase alteration of the oscillation during scanning in the tapping mode AFM is sensitive to changes in material property, particularly variations in mechanical properties. Because the modulus of the inorganic nanoparticles is typically greater than that of a polymer, the nanoparticles can be visible in an AFM phase image. LSCM was performed using a Zeiss model LSM510 (Carl Zeiss Microscopy, Thornwood, NY, USA) and a laser wavelength of 543 nm. The images were taken at magnifications of 5× and 50×, with an optical slice (*z*-step) of 0.1 µm.

The chemical degradation and transformations at and near the sample surfaces as a function of UV dose were followed by ATR-FTIR and XPS. ATR-FTIR spectra were collected using a spectrometer (Nexus 670 Spectrometer, Thermo Nicolet, Madison, WI, USA) equipped with a liquid nitrogen-cooled mercury cadmium telluride (MCT) detector, a ZnSe prism and an incident angle of 45°. These parameters resulted in a probing depth mostly within the 2.5-µm material layer from the exposed surface, as specified in the Supplementary material. All spectra were the average of 128 scans and recorded at a resolution of 4 cm^{-1}. For each exposure dose, the results were the average of nine spectra collected on three different specimens. The peak height was used to represent the IR intensity, which is expressed in absorbance (*A*).

XPS was performed on an Axis Ultra DLD spectrometer from Kratos Analytical (Spring Valley, NY). Samples were mounted onto a samples bar and loaded into an ultra-high vacuum (UHV) chamber for spectra acquisition ($P_{base} < 10^{-9}$ torr). Monochromatic $Al_{K\alpha}$ X-rays were employed at 150 W and photoelectrons were collected at a vector along the surface normal with the charge neutraliser running. Spectra were acquired in wide survey scans (1300 eV range) with photoelectrons collected at a pass energy of 160 eV at 1 eV per step. Each UV irradiated sample was measured in triplicate at different points on the sample. Elemental analysis was performed using *CasaXPS* (Teignmouth, UK) using a Shirley background fit for each elemental region. All spectra were energy adjusted based on shifting the C 1s peak maximum to a value of 285 eV representative of the hydrocarbon contributions. Elemental sensitivity factors provided by Kratos were 0.477, 0.278, 0.78, 1, 0.193 and 0.328 for the N 1s, C 1s, O 1s, F 1s, Al 2p and Si 2p photoelectrons respectively. Except for the 386 MJ m^{-2} dose (32 days) where only two measurements were made, values reported and plotted from 12 (1 day) to 290 MJ m^{-2} (24 days) of UV irradiation were representative of the average of the 3 measurements ± 1 standard deviation.

The aging by SPHERE was included to challenge the ISO-standardised equipment with a different set of aging parameters in a unique, yet highly established and controlled setup. Additional uncertainties were linked to the immersion sampling of release as described below.

Induced release by UV + immersion sampling method at BASF, for specimen weathered at LEITAT, NIST or BASF

The combined action of matrix degradation and mechanical stress in the presence of water was previously assessed on thermoplastic polyurethane (PU) containing 3 mass % carbon nanotubes (CNTs) as a first exploratory test case for nanomaterial release from polymer nanocomposites exposed to UV radiation.[18] The protocol was further refined for the current study as described below and in Table 1. To assess actual release from 12 specimens, each weathered piece with a surface area of 42 to 55 cm^2 was immersed in a surfactant solution (3.5 mL H_2O + 0.5 g L^{-1} sodium dodecyl sulfate, SDS) in 50-mL bottles with a closed lid. The irradiated surface was downwards oriented to ensure its immersion despite the low liquid volume. Such aged polymer samples were not flat, so that they were in contact with liquid and could not adhere to the glass. A minimal immersion liquid volume was chosen because at a given limit of quantification in the colloidal state (mg mL^{-1}) the immersion volume linearly translates to the limit of quantification per irradiated surface area (mg m^{-2}). To simulate release into waters without mechanical forces, the bottle was left standing for 24 h before the first aliquot of 0.5 mL was withdrawn for analysis. To simulate continued outdoor use with mechanical stresses, the bottles were then placed on a shaker for 24 h (Vibrax VXR, IKA, Staufen, Germany, operating at 5 Hz with 5-mm amplitude) and the next aliquot was withdrawn for analysis. As a worst-case analysis without corresponding real-world scenario, the bottles were finally placed in a sonication bath for 1 h, before the last aliquot was obtained.

Compared to real-world rain or surface waters, which may contain interface-active substances, dusts and other atmospheric pollutants, the addition of surfactant during the immersion and induced release was intended to minimise an underestimation of the probability of release, because a quantitative validation against real-world outdoor run-off waters was not available.

The presence of surfactant was essential to keep fragments dispersed, so that they could be quantified in size-selective intervals. Fractionating techniques such as field-flow-fractionation (FFF) or analytical ultracentrifugation (AUC)[24,25] are especially suited to quantify traces of colloids within a heterogeneous mixture. AUC was validated for this purpose by deliberately mixed calibration beads[24] and deliberately mixed free nanofillers in a 200-fold excess of polymer degradation fragments.[18] Here we used interference optics (Beckman model 'XLI proteome laboratory') and the raw data was fitted by the free-ware software *SedFit* ver. 14.0 (Peter Schuck, see http://www.analyticalultracentrifugation.com) using the refractive index increment of SiO_2: $dn/dc = 0.063$ cm^3 mg^{-1}. The mass concentrations of fragments were read directly from the interference fringe shift without further conversion. The limit of detection was 50 mg L^{-1} as defined by comparing freely dispersed SiO_2 against a water blank.[24] For each aliquot, the mass-concentration of fragments was determined in the size interval below 150 nm, where also free nanofillers would be expected, and in the particle sizes up to ~5 µm. The AUC analysis used at least two measurements for one data point, which represented ~10^9 particles. The content of fragments was referenced to the water volume used to induce

release (3.5 mL) and to the irradiated polymer surface, and is thus given in units of milligrams per square metre.

To prepare for TEM and EDX analysis, the surfactant was washed by centrifugation at 250 000*g* for 4 h (ensuring that fragments down to 2 nm were retained) and redispersion in pure water. The fragments were then characterised by TEM (FEI, Type Strata 400 DB) equipped with a field emission cathode.

For one sample irradiated at NIST with 833 MJ m^{-2}, we modified the protocol to enhance the simulation of real-world outdoor release: the entire protocol to induce release (immersion + shaker + sonication) was performed in ultrapure water. Aliquots were withdrawn for TEM shape and size analysis without further preparation. For mass concentration and size analysis by AUC, a drop of SDS solution was added to the aliquot to obtain the same final SDS concentration as above (0.5 g L^{-1}), bath-sonicated for 5 min to de-agglomerate and then measured by AUC.

Results and discussion of aging and release protocols

Characterisation of nanocomposite surface morphology exposed to UV radiation

The mass loss of neat PA and the PA–nanosilica composite as a function of UV dose (at NIST) is displayed in Fig. 1. The mass loss is expressed as [(initial mass − mass at a particular UV dose)/initial mass] × 100. Except for some fluctuation at the very low dose (early exposure), the mass loss of both neat PA and the PA nanocomposite was nearly linear with UV dose. The small fluctuation at the very early exposure stage was probably due to the instability of RH in the exposure chamber before it reached equilibrium.

Fig. 1 shows that both the rate and amount of mass loss of the PA–nanosilica composites were essentially the same as those of the neat PA. Both materials lost ~2.5 % of their mass after irradiating with a UV dose of 833 MJ m^{-2}. Despite clear evidence of a substantial accumulation of silica nanoparticles on the PA nanocomposite surface at this dose (see AFM images in Fig. 2) and the fact that the density of silica is almost two times greater than that of the polymer (2.2 *v.* 1.12 g cm^{-3}), the result of Fig. 1 suggests that little or no nanosilica was released in the dry state[5,21] from the PA nanocomposite after 833 MJ m^{-2} of UV irradiation.

Under UV radiation, polymer nanocomposites generally undergo a substantial surface morphological change, which includes accumulation of silica nanoparticles on the sample surface.[4] Tapping mode AFM was employed to follow these morphological changes of PA nanosilica composite as a function of UV dose. Fig. 2 displays AFM images of neat PA and the PA–nanosilica composite for different UV doses. The surface of neat PA before UV exposure (0 dose) was rougher than that of its nanocomposite counterpart. The roughness if the PA nanocomposite is higher for intermediate UV doses, before the roughnesses of neat PA and the PA nanocomposite level out at the highest UV doses, probably dominated by cracking (Fig. S8). The crystalline structure of PA is visible in the AFM images of both neat PA and PA nanocomposite samples. In addition, AFM images of the unexposed nanocomposite show the presence of particles having sizes in the nanometre range (top right). These nanosize particles are probably clusters of spherical silica nanoparticles. As seen in Fig. 2, the number of spherical nanoparticles increased as the UV dose increased. After an accumulated UV dose of 833 MJ m^{-2}, a substantial amount of nanosilica particles has covered the PA nanocomposite surface. The repeated AFM measurements on the same

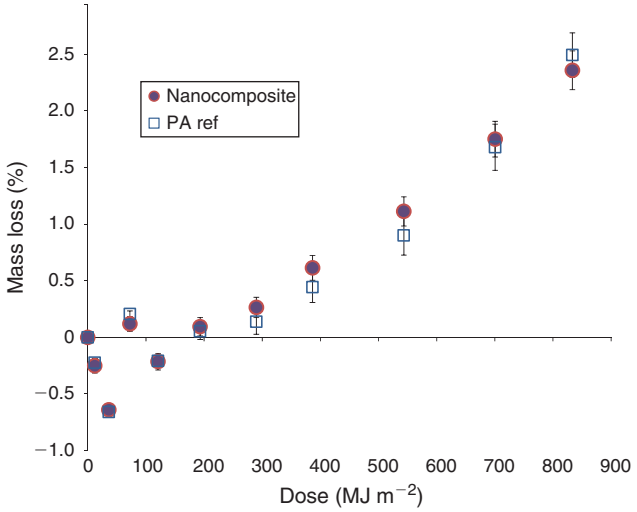

Fig. 1. Mass loss *v.* dose for neat polyamide (PA) (open box) and PA–nanosilica composite (filled dot) irradiated with UV at 65 °C and 50 % relative humidity (RH). Each data point was the average of four samples, and error bars represent one standard deviation.

samples at various UV doses (irradiated and measured at NIST) were confirmed by SEM measurements on samples withdrawn at the same dose or time intervals (irradiated at NIST or at BASF, measured at BASF) shown in Fig. S7. The identification of particle structures as nanosilica is supported by backscatter electron imaging, thus highlighting the inorganic particles as bright spots. Fig. S7 suggests that after a dose of 145 MJ m^{-2} the nanosilica particles are mostly still *in* the PA matrix, whereas from 435 MJ m^{-2} some particles remain *on* the surface that has now further receded, with more particles just emerging from the polymer matrix. After 833 MJ m^{-2} or at the higher UV doses and still without rain, the remaining surface consists entirely of nanosilica particles. Interestingly, after UV + rain weathering only a few particles are observed loosely *on* the surface, but nanosilica particles are clearly identified by their structure and electron backscattering *in* cracks of the topmost layer of the degraded nanocomposite.

For neat PA, as the amorphous phase is removed by the photodegradation (because of its higher oxygen permeation than the crystalline phase), a needle-like structure became the dominant surface feature after ~193 MJ m^{-2} UV irradiation. This is more easily seen in the higher spatial resolution AFM phase image (Fig. 2a, middle row, right inset) and in the SEM scans (Fig. S7). The needle-like structure is commonly observed on the PA surface irradiated with UV radiation and is attributed to the chemi-crystallisation process, in which entangled molecules in the amorphous phase undergo chain scission and the cleaved polymer chains that are free of entanglements tend to crystallise.[26]

In addition to AFM, LSCM was used to characterise surface morphological changes of the PA nanocomposite irradiated with UV light. Although LSCM does not have the spatial resolution to characterise nanosize features occurring on the polymer nanocomposite surface during aging, it can provide macroscopic changes of these advanced materials that may be useful for relating to surface accumulation and release of nanoparticles. Fig. 3 displays LSCM images at two magnifications for neat PA and the PA–nanosilica composite as a function of UV dose. Both unexposed neat PA and unexposed PA–nanocomposite samples show the presence of some bright

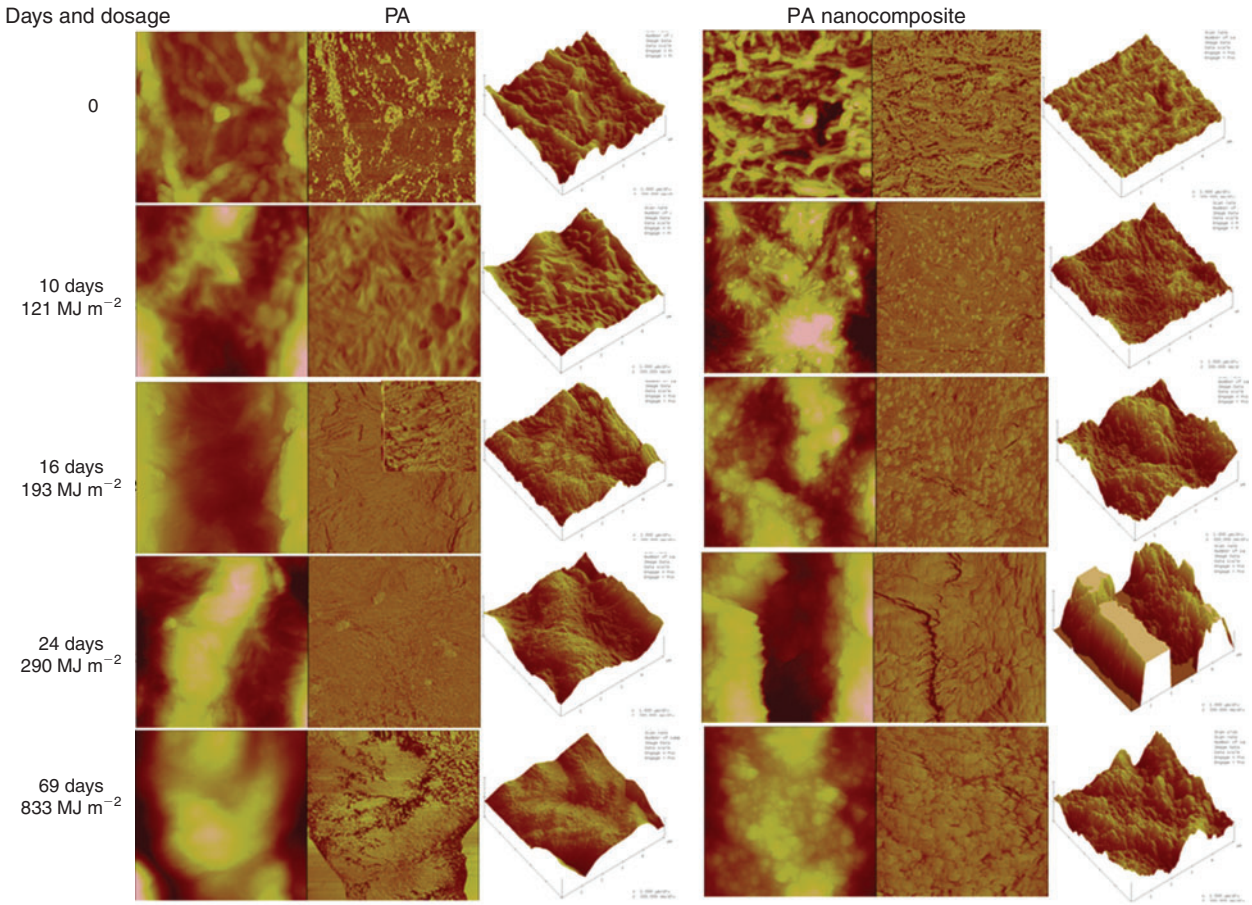

Fig. 2. Atomic force microscopy (AFM) height and phase images of neat PA and PA nanosilica composite as a function of UV dose. For each AFM pane, the 2-D height image is on the left, 2-day phase image is in the middle and 3-D height image is on the right. The scan size of all AFM images is 5 μm, the *Z* division of all 3-D images is 300 nm, and the inset scan size is 1 μm. Quantitative evaluation of roughness changes as a function of UV dose as displayed in Fig. S8.

spots (due to particles raised above the surface) on their surfaces (reflexion mode). After irradiation at a dose of 72 MJ m^{-2}, numerous cracks have appeared in the neat PA sample, but no evidence of cracks was visible in the PA nanocomposite at this UV dose. This result suggests that it took a longer time or a higher UV dose for cracks to develop in the PA nanosilica composite as compared to that in the neat PA. Fig. 3 shows that a network of mud cracks has formed in both materials at a dose of 121 MJ m^{-2}, and the crack density and size (i.e. crack width) increased with increasing UV dose. At the highest dose (833 MJ m^{-2}), a substantial surface area of both materials was occupied by cracks. This can also be seen in the low magnification SEM image in Fig. S7.

In addition to a difference in the UV energy level required for cracks to develop, there are two distinctive differences in the crack properties between the neat PA and the PA–nanosilica composite. At the same UV dose, both crack length and crack width of the nanocomposite appeared to be shorter and narrower than those of the neat PA. These differences are better observed in the LSCM images at the 121 and 290 MJ m^{-2} doses, where the cracking was extensive but crack dimensions were still distinguishable. Cracks in the nanocomposite appeared to terminate after travelling a short length, whereas those in the neat PA propagated a long distance before termination. Because cracks in the PA material generally initiate from the centre of the spherulites,[26] these noticeable differences suggest that the incorporation of silica nanoparticles in the PA matrix has altered the microstructure of this polymer, as evidenced also by the spherulite structures in the SEM scans (Fig. S7).

Characterisation of the chemical changes after UV aging

In this study, ATR-FTIR and XPS were used to follow the chemical degradation of neat PA and PA nanosilica composite as a function of UV dose. As presented in Fig. S1, except for a broad band in the 1000–1250 cm^{-1} region, the ATR-FTIR spectrum of the unexposed PA–nanosilica composite is similar to that of the neat PA. It shows the main bands at 1640 cm^{-1}, due to hydrogen-bonded C=O (amide 1), at 1538 cm^{-1} attributed to mostly NH and CN (amide II)[27] and 2928 cm^{-1}, due to C–H. Based on the FTIR spectroscopic characteristics of neat PA (Fig. S1) and silica nanoparticles (Fig. S2), we assigned the broad band in the 1000–1250 cm^{-1} region of the unexposed PA–nanosilica composite as due mainly to the Si–O bonds.

We have utilised a FTIR difference spectroscopy method, where gain or loss of a functional group can be readily discerned, to follow the chemical degradation of neat PA and its nanosilica composite as a function of UV dose. Fig. S5 displays difference ATR-FTIR spectra of neat PA and the PA–nanosilica composite for several UV doses. These spectra were obtained by subtracting the spectrum of the unexposed specimen from those recorded at different UV irradiation doses of the same specimen.

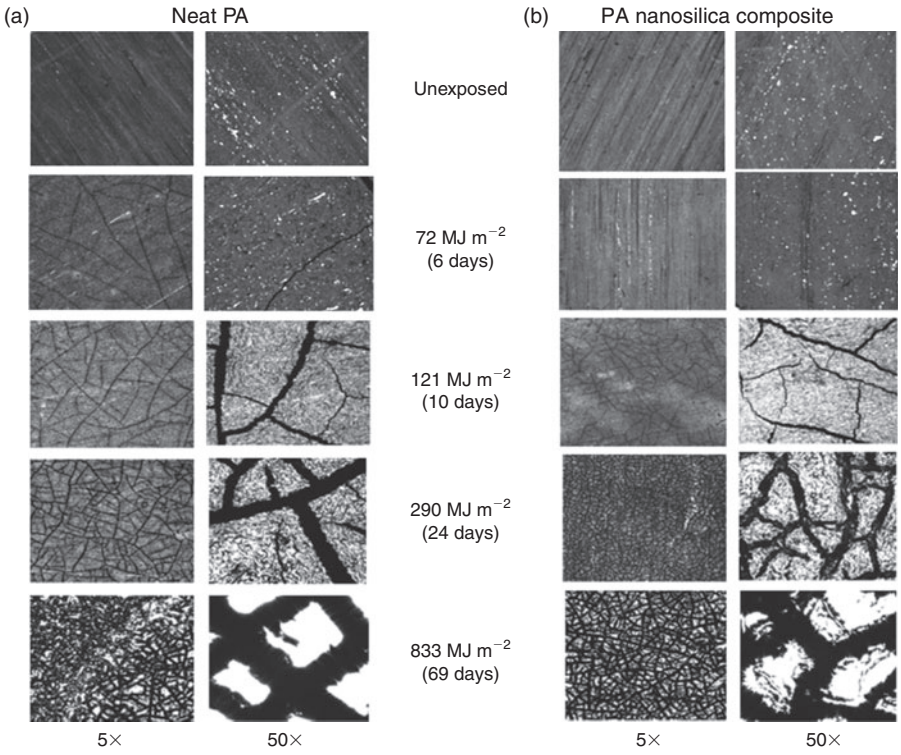

Fig. 3. Laser scanning confocal microscopy (LSCM, reflexion mode) images at two magnifications of neat polyamide (PA) (a) and PA–4 % nanosilica composite (b) as a function of UV dose, showing that UV radiation induced a mud cracking pattern in both materials and that the cracking density increased with increasing UV dose.

Before the subtraction, all spectra were normalised against the least-changed band at 929 cm^{-1} to account for any concentration effects from differing sampling efficiency. In a difference spectrum, bands below and above the zero absorbance line respectively represent a loss (e.g. chain scission) and a gain (e.g. oxidation) of a functional group in the sample. As shown in Fig. S5, the intensities of numerous bands of the PA matrix and its nanosilica composite have substantially decreased, such as the bands at 1640, 1538, 2928 and 3280 cm^{-1}. In addition, new strong bands at 1688 and 1708 cm^{-1}, respectively attributed to imide (CO–NH–CO)[14,16] and the C=O group of carboxylic acids, have appeared. The formation of these oxidised products suggests that the degradation of neat PA and the PA–nanosilica composite under the UV condition used in this study followed a similar photo-oxidation mechanism described in the literature for this polymer.[14,16] Detail regarding the photodegradation mechanism of PA is beyond the scope of the present study but can be found in the above references. Both the neat PA and the PA–nanosilica composite samples also showed increasing yellowing with increased UV dose, suggesting that a substantial amount of conjugated structures had formed in the PA matrix. Such conjugated chemical structures readily absorb UV radiation and can initiate photochemical reactions.

The bands at 1538, 1708 and 1048 cm^{-1} (respectively assigned above to mainly NH + CN, carboxylic acid C=O and Si–O bonds) were respectively used to follow chain scission, oxidation and surface accumulation of nanosilica particles of the PA–nanosilica composite during exposure to UV radiation. Fig. 4 depicts intensity changes of these three bands with UV dose for both neat PA and PA nanocomposite. Both the PA and its nanosilica composite underwent rapid photodegradation with extensive chain scission and formation of a substantial amount of oxidised products with UV exposure. Both the rate and degree (magnitude) of chain scission of the PA nanosilica composite were noticeably greater than those of the neat PA (Fig. 4a). A similar trend was observed for the bands at 1640 (amide C=O) and 2928 cm^{-1} (CH_2) (not shown). However, the intensity change of the oxidation with UV dose was quite different from that of the chain scission process. For the dose from zero to 193 MJ m^{-2}, the oxidation followed a similar trend with the chain scission. That is, both the rate and degree of oxidation of the PA–nanosilica composite were greater than those of the neat PA. However, whereas oxidation of the PA nancomposite essentially reached a plateau after the 193 MJ m^{-2} dose, this degradation process of the neat PA rose rapidly thereafter.

Similar behaviour was also observed for other bands due to oxidised products such as at 1688 (due to CO–NH–CO) and 1760 cm^{-1} (due to lactone) (not shown). This result suggests that an accelerating oxidation process has occurred in the neat PA matrix after it has been irradiated in the SPHERE to a certain UV dose. Why such a process was absent in the PA nanosilica composite is unknown. One possibility is, under UV light, some fractions of the silane layer covering the silica nanoparticles were degraded, and the unprotected, hydrophilic silanol sites on the silica nanoparticles readily adsorbed the polar chromophores that were formed by the oxidation of PA, such as hydroperoxides and carbonyl compounds. The strongly adsorbed chromophores on the Si nanoparticles were probably less effective for repeating the initiation and photo-oxidation processes in PA.

The intensity change of the band peaking at 1048 cm^{-1} was used to follow the accumulation of nanosilica particles on the nanocomposite surface as a function of UV dose. Before exposure, this band was absent in the spectrum of neat PA but visible

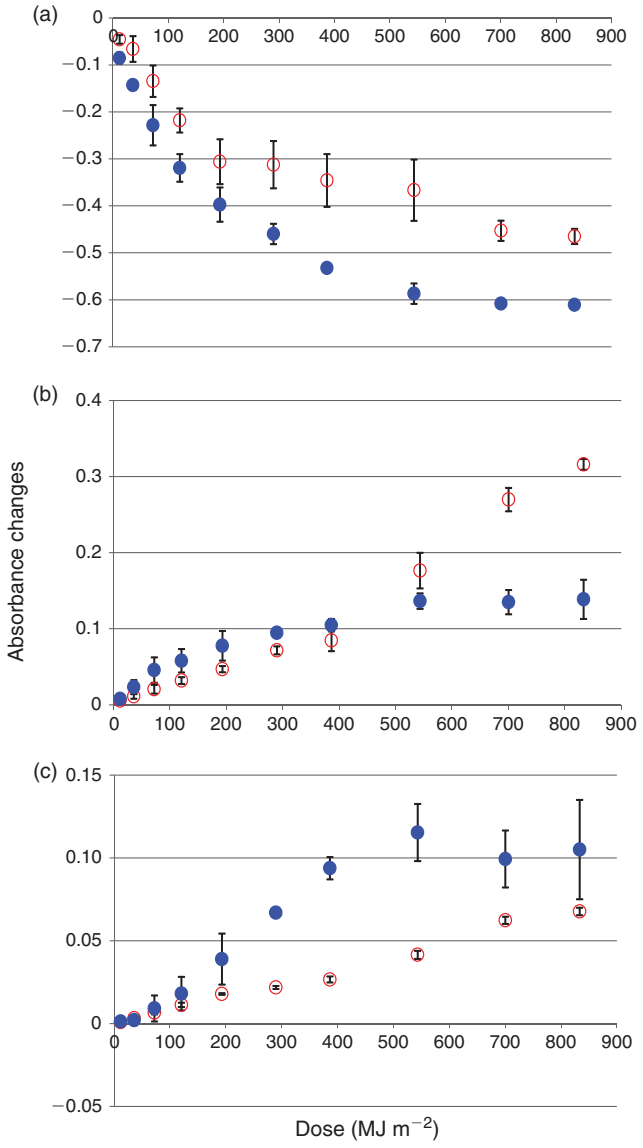

Fig. 4. Attenuated total reflection Fourier-transform infrared (ATR-FTIR) intensity changes with UV dose for: (a) 1538, (b) 1708 and (c) 1048 cm^{-1} bands for neat polyamide (PA) (open symbol) and PA_nanosilica composite (filled symbol). Each data point was the average of nine spectra from three specimens, and the error bars represent one standard deviation.

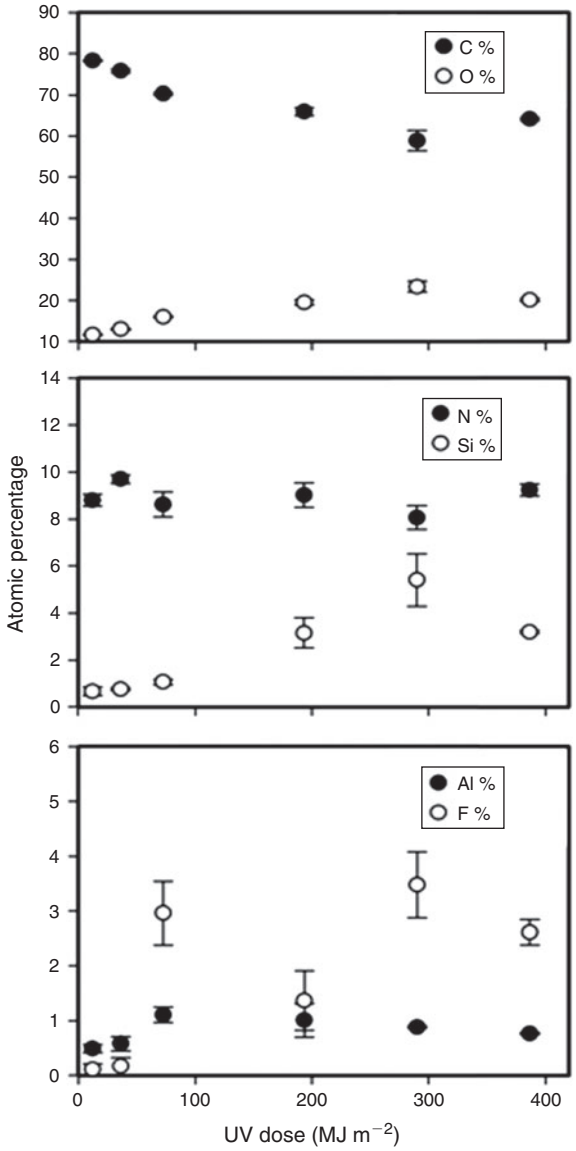

Fig. 5. X-Ray photoelectron spectroscopy (XPS) derived atomic percentages *v.* dose of PA nanosilica composite irradiated with UV.

in the spectrum of its nanosilica composite (Fig. S1). However, it is interesting to note that the intensity of this band of the neat PA also increased with increasing UV dose (Fig. 4c). This increase in the neat PA material was likely due to formation of oxidised products containing the ether bonds (C–O), such as hydroperoxides (C–OOH) and primary alcohols (CH_2–OH). The C–O stretching of these compounds appears in this region.[28] For the UV-irradiated PA–nanosilica composite, the intensity increase of this band, which is a summation of the Si–O and C–O bonds, with increasing UV dose was greater than that of the neat PA (Fig. 4c). This larger intensity change for the nanocomposite is attributed to the increase of the Si–O bonds from the nanosilica particles accumulated on the sample surface resulting from UV exposure. This postulation is supported by XPS data (Figs 5, S6) and AFM images (Fig. 2), and is consistent with previous studies of UV irradiation of epoxy nanosilica composites.[29,30] Furthermore, the intensity of the 1048 cm^{-1} band decreased at the two highest UV doses. This decrease was probably due to the extensive cracking occurring in the UV-irradiated samples as seen in the LSCM images (Fig. 3). The presence of large cracks in the sample surface will decrease the amount of nanosilica particles in contact with the ATR prism.[14,16]

XPS elemental analysis of the PA–nanosilica composite as a function of UV dose is plotted in Fig. 5, and representative spectra are provided in Fig. S6. At low UV doses, the spectra were almost completely dominated by the C 1s, O 1s and N 1s elemental regions (see top and middle plots in Fig. 5). This is consistent with a surface layer dominated by the PA polymer, with only a low concentration of silicon being observed, as has been reported for different polymeric-like matrix materials such as epoxy.[29,30] Indeed, the contributions of the Si 2p region were vanishingly low at 12 MJ m^{-2} (middle plot, Fig. 5). Although the resolution of this study is insufficient to definitively identify

Table 2. Mass balance of fragments recovered from run-off waters of UV + rain weathering (the number in parenthesis represents one standard deviation ($n = 4$)

Specimen	Run-off water total volume (L)	Concentration in run-off water (mg L^{-1})	Total release (mg)	Release per specimen surface (g m^{-2})
Neat polyaminde (PA)	91.7 (0.1)	4.3 (0.4)	403 (38)	6.8 (0.6)
PA–nanosilica composite	62.5 (0.1)	6.1 (0.5)	379 (31)	6.4 (0.5)

different chemical states, other results suggest that a composite that contains Si 2p at the surface is typically due to silanising agents, consistent with previous studies.[30] Additionally, a close examination revealed the presence of trace amounts of F 1s and Al 2p photoelectrons (Fig. 5c).

As the UV irradiation dose increased, the C 1s decreased and the O 1s increased in percentage composition. This is in agreement with a photo-oxidative degradation, which is common in polymeric materials exposed to UV radiation (Rabek 1995). The N 1s region, however, did not significantly change throughout the entire UV irradiation doses, maintaining an average of 8.89 ± 0.64 % throughout the duration of the study (average and standard deviation representative of 17 measurements across all UV doses measured). The Si 2p percent contribution made statistically significant increases, starting at a dose of 72 MJ m^{-2} and continued to increase to a value of 5.40 ± 1.11 % before dropping back down to a value of 3.19 ± 0.06 %. This surface enhancement of the silicon concentration is consistent with previous results,[29,30] providing further evidence of the photo-oxidative degradation of the composite surface, resulting in removal of the PA matrix and leaving the nanosilica particles at the surface. The drop in Si concentration at the highest UV dose in Fig. 5b may be due to the extensive cracking as shown in Fig. 3.

The trace contributions of aluminium and fluorine also increased with UV irradiation, albeit not always in a consistent manner for fluorine. The Al 2p contributions had a much more systematic increase followed by a decrease in surface concentration, increasing steadily to a maximum at a UV dose of 72 MJ m^{-2} before slowly falling to a final value.

The fact that the F increases with the Si surface concentration suggests that it may be associated with the silica nanocomposite, either in the form of surface contamination or as part of a surface functionalisation to enhance the particles ability to mix into the PA. The systematic decrease of the Al contribution in the second half of irradiation supports its attribution to a contamination from the Al foil used during melt pressing of the plates from pellets.

Quantification of spontaneous release during aging v. induced release after aging

After completing the accelerated aging process of the samples, water run-off samples collected from the weathering apparatus at LEITAT were analysed by different techniques. Before the analyses, released materials were first isolated by lyophilisation (freeze-drying process). No material could be recovered from the empty position of the weathering apparatus used as control. The materials recovered for the neat PA and the PA nanocomposite samples are given in Table 2. The section *UV exposures, sampling and characterisation at LEITAT, Spain* and Table 1 provide details on the UV–wet cycle exposure conditions and the procedures for obtaining the release material results given in this table. The results are the average of three samples.

The results of Table 2 suggest that, under the accelerated weathering conditions used specified in as above of this study, there was little difference in the amounts of material release between the neat PA and the PA–nanosilica composite (6.8 *v.* 6.4 g m^{-2}). This result is consistent with the mass loss data displayed in Fig. 1. Furthermore, the release value of 6.8 g m^{-2} after a dose of 216 MJ m^{-2} can be expressed as 31 mg MJ^{-1} as a rule of thumb for unstabilised PA material (Table 3), assuming a linear relationship between UV dose and release mass, similar to that of Fig. 1 obtained for samples exposed to UV in the NIST SPHERE. In order to assess how fragments were released from neat PA and the PA nanocomposite, we employed three induced release methods for sampling as specified in Table 1. Fig. 6 depicts the release amounts by the maximum shear-induced method (sonication) as a function of UV dose for two UV intensities. These results are from samples UV-irradiated without rain at NIST or at BASF. The results are reproducible and can be fitted by a power law with the parameter summarised in Table 3.

For comparison, the gravimetrically determined spontaneous release during accelerated weathering with rain (red cross) was above either of the dry aging and immersion release protocols. Compared to the induced release by immersion after aging at the same ISO-specified lamp source and same 60 W m^{-2} intensity, the spontaneous release during weathering was a factor 20 higher. This result is reasonable, because (a) the matrix likely degraded at a faster rate during exposure to water and UV (PA is sensitive to hydrolysis as indicated in the introduction) than for exposure to UV alone and (b) the gravimetric detection of the entire solid content is more inclusive than the AUC quantification of submicrometre particles only. The extent of disagreement on the release rates (quantities) is significant, and is summarised by the value of release per UV dose (Table 3, in units of milligrams per square metre per megajoules per square metre or milligrams per megajoule).

We have also investigated the relationship between spontaneous release and induced release and the effects of the shear energy during immersion on the release results. Fig. 7 summarises the effects of rain, UV dose and shear energy on the amounts of release material for both the neat PA (blue) and the PA–nanosilica composite (red). Overall, the red and blue bars follow the same trends and are identical within the error bars, confirming the result from surface characterisation that the presence of nanosilica did not significantly influence the PA degradation. Fig. 7 also revealed that the dependence of release amounts on shear energy during immersion was weak. The considerable scatter in some cases appeared to obscure a general trend of increasing release fragments from unmoving immersion to shaker treatment to sonication treatment. Also, for the highest UV dose of this report (NIST, 833 MJ m^{-2}), where the surface

Table 3. Release results depending on protocols

Protocol according to Table 1	Release characteristics	Release quantity	Remarks
Dry aging (ISO4892-2), release sampling by immersion	Polydisperse mixture of predominantly composite fragments, (irregularly shaped), from the nanoscale up to several micrometres in diameter, and occasionally of clustered or free nanosilica. (Figs 8–10, Figs S10–11)	Approximately 0.6 mg MJ^{-1}. Same for neat PA and PA nanosilica composite (Fig. 7, Fig. S9)	(mg m^{-2}) = 0.19 × UV dose (MJ m^{-2})$^{1.2}$ (fit to Fig. 6). Release quantity increases 50 % from zero to maximum shear forces
Wet aging (ISO4892-2), 18 min/102 min, release sampling by immersion		Approximately 0.5 mg MJ^{-1}. Same for neat PA and PA nanosilica composite (Fig. 7, Fig. S9)	No critical dependence on details of wet/dry cycles
Wet aging (ISO4892-2), 1 min/29 min, release sampling by immersion		Approximately 0.5 mg MJ^{-1}. Same for neat PA and PA nanosilica composite (Fig. 7, Fig. S9)	
Wet aging (ISO4892-2), 1 min/29 min, release sampling from run-off waters		Approximately 31 mg MJ^{-1}. Same for neat PA and PA nanosilica composite (Table 2, Fig. 7, Fig. S9)	Two orders of magnitude more release quantity due to hydrolysis of PA
Dry aging (SPHERE), release sampling by immersion		Approximately 4 mg MJ^{-1}. Same for neat PA and PA nanosilica composite, except 833 MJ m^{-2} + sonication (Fig. 7, Fig. S9)	(mg m^{-2}) = 0.12 × UV dose (MJ m^{-2})$^{1.7}$ Critical dependence on aging conditions

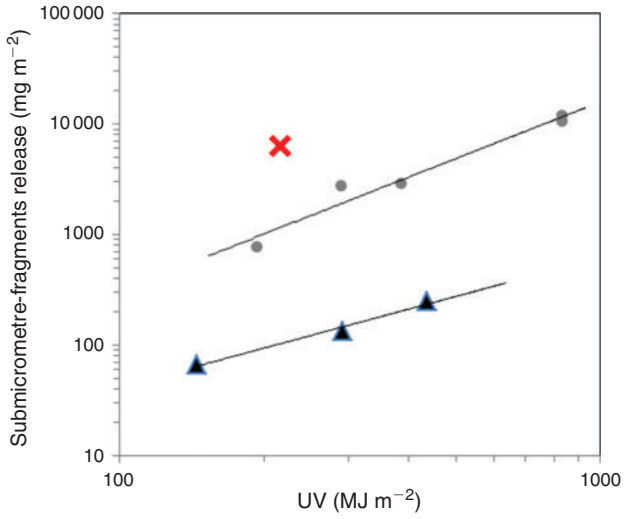

Fig. 6. Quantification of release from the polyamide (PA)–nanosilica composite. Samples UV-irradiated without rain at NIST (grey dots) or at BASF (black triangles), were subjected to shear induced release sampling by the immersion + sonication method, and the size-fractionated content of submicrometre fragments in water was quantified by analytical ultracentrifugation (AUC). All fragments below 1-µm diameter were included, which represent the dominating size fraction. The error of AUC measurement is approximately the same size as the symbol size. Immersion and measurement were performed using one sample, except for the highest UV dose where the results of two samples are shown and overlap within the symbol size. The parameters obtained for the power law fits are given in Table 3. The red cross indicates the gravimetrically determined spontaneous release during UV + rain weathering (at LEITAT). See Tables 1 and 3.

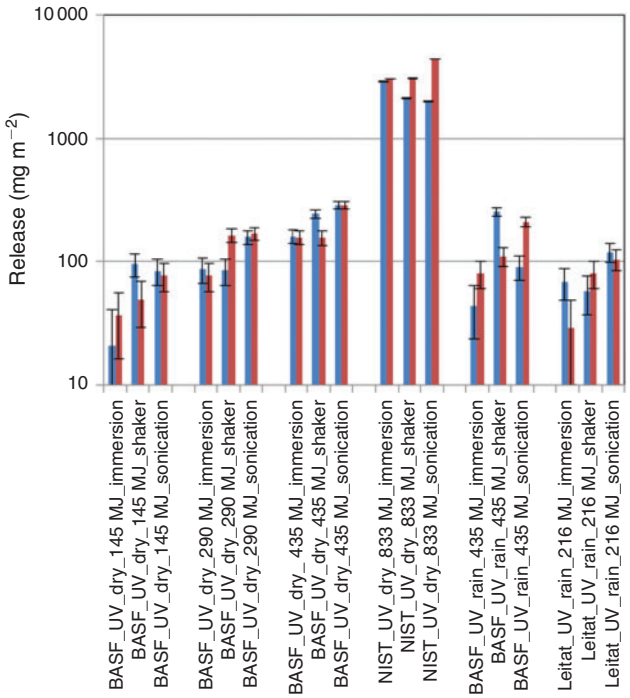

Fig. 7. Quantification of release induced by immersion with gradually increasing shear. Blue bars, neat polyamide (PA); red bars, PA–nanosilica composite. The analytical ultracentrifugation (AUC) measurement includes size fractionation, and shown here is the range of fragments with sizes below 150-nm diameter. The systematic error bar represents the quantification of sub-milligram solid content diluted in 3 mL of immersion fluid by AUC. Reproductions, negative controls and micrometre-sized fragments are included in Fig. S9.

of the PA–nanosilica composite was found to consist entirely of the remaining nanosilica, the submicrometre release from the nanocomposite showed the same slight increase with increasing shear.

Interestingly, submicrometre fragments can also be released by immersion, shaking or sonication from samples that had undergone rain cycles during UV irradiation. Comparing different rain cycles (Table 1), the higher amount of released

fragments from the samples aged by ISO 4892 at BASF correlated exactly to the doubled UV dose (BASF 435 MJ m^{-2} *v.* LEITAT 216 MJ m^{-2}). The fact that the samples at LEITAT were sprayed with water during 3 % of the aging time, compared to 15 % of the aging time at BASF, could have left a higher amount of nanosilica on the surface; however, this effect was not observed (Table 3).

Additional data on micrometre-sized fragments is presented in the Supplementary material (Fig. S9) where we also include complete reproductions of rain cycle aging by both LEITAT and ISO protocols, immersion and quantification. The data showed that the measurements are reproducible within 30 % absolute error, which we estimated to be dominated by the quantification step, which required the measurement of some micrograms of fragments diluted in 3 mL of immersion water. Micrometre-sized fragments tended to be more pronounced in samples of severe polymer degradation, such as from wet weathering or high UV doses. Micrometre-sized fragments decreased with mild shear (shaker) and then increased again with maximum shear (ultrasonication) (Fig. S9). This observation points to the possibility that shear can break fragments into smaller pieces, so that the mass in the micrometre-range decreases, concomitant with the observed increase of smaller fragments (Fig. 7).

Identification of release morphology

Recovered materials both from the collected run-off waters (at LEITAT) and from the immersion waters with induced release (at BASF and on samples weathered at NIST, LEITAT, BASF) were imaged by TEM, and a gallery of morphologies obtained is presented in Figs 8–10 and Figs S10 and S11. Within TEM analysis, EDX spectroscopy and dark field EM was used to identify Si-containing fragments. For enhanced representation and statistics, the results of few fragments in TEM were complemented by FTIR and TGA chemical characterisation of large ensembles of many fragments.

Care must be taken to identify release fragments by morphology only or by chemical composition only, because the neat PA did also release small fragments that may resemble nanofillers. However, a combination of microscopy and spectroscopy can provide useful information for identifying nanofiller and polymer fragments (Fig. S10).

Release fragments were extremely polydisperse, ranging from large structures with complex shapes and diameters above 10 µm down to clusters of inorganic particles on the order 10 to 100 nm. This observation applied to both spontaneous release during UV + rain weathering (Fig. 8), induced released by immersion after UV irradiation (Fig. 9) and induced release by immersion after UV + rain weathering (Fig. 10). Comparing composition and size, we did not observe a significant difference between the fragments of spontaneous or induced release (Fig. 8 *v.* 9). We also did not observe a general trend of fragment composition with UV dose (Figs 9, 10). It appears that the elongated above-20 µm structures only emerged from the lowest UV doses in dry weathering (Fig. 9), but the polymer–nanosilica composite remained the dominating type of fragments for any UV dose, and their size does not change by any obvious trend, although the effects may be concealed by the limited statistics from TEM images. We finally examined to what extent our immersion protocol with SDS surfactant in water influences the properties of released

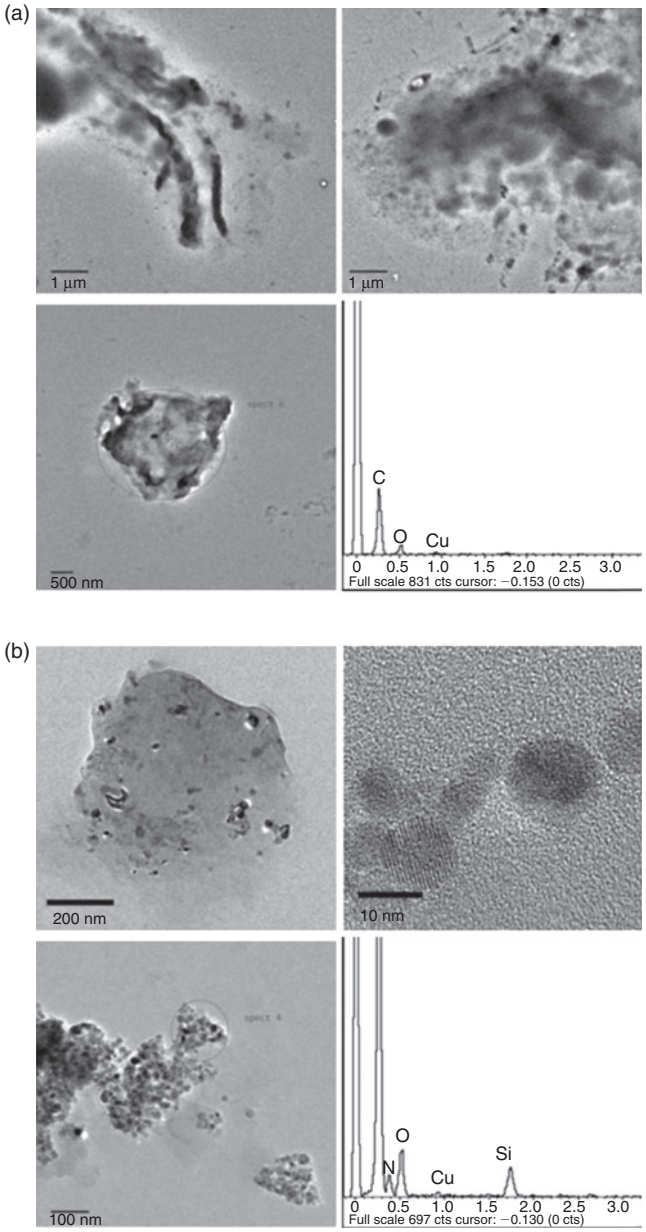

Fig. 8. Transmission electron microscopy (TEM) of spontaneous release fragments sampled from run-off waters at LEITAT from neat polyamide (PA) (a) and PA–nanosilica composite (b) (1/29 min wet/dry protocol): nanoparticles can be visualised clearly in the images of the nanocomposite fragments; the presence of Si in the nanocomposite fragments release from PA nanosilica composite was confirmed by energy-dispersive X-ray spectroscopy (EDX). In general, the released material obtained was a mixture of isolated nanosilica, nanosilica embedded within polymer material, and polymer material alone.

fragments. We found that there was no difference in fragment structures or morphology with or without SDS surfactant during immersion (Figs 9, S11).

Identification of release composition

In the case of fragments released into run-off water samples during the UV + rain aging of a neat PA specimen, TEM characterisation (Figs 8a, S10) suggested the presence of mainly organic matter. However, in some regions, EDX spectra

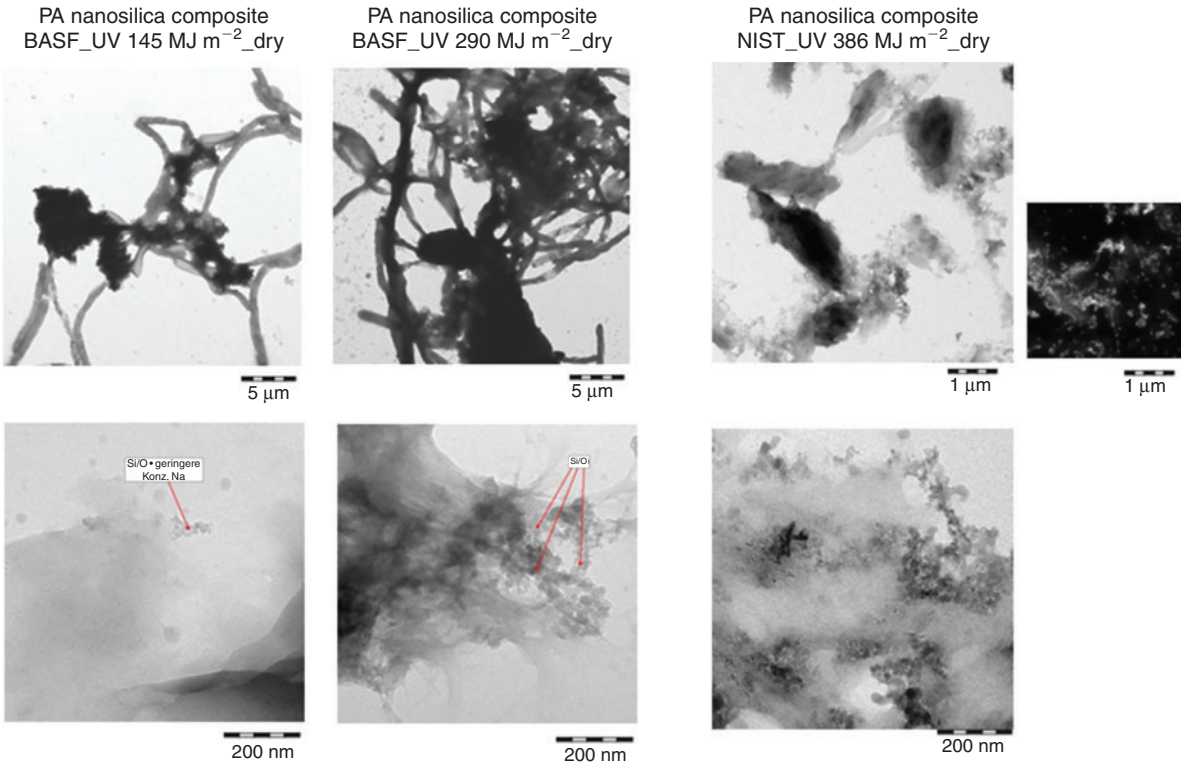

Fig. 9. Transmission electron microscopy (TEM) of induced release fragments from polyamide (PA) nanosilica composite (UV irradiated at BASF or NIST, immersion and release at BASF). Dark field TEM identified Si-containing structures throughout the larger and smaller fragments.

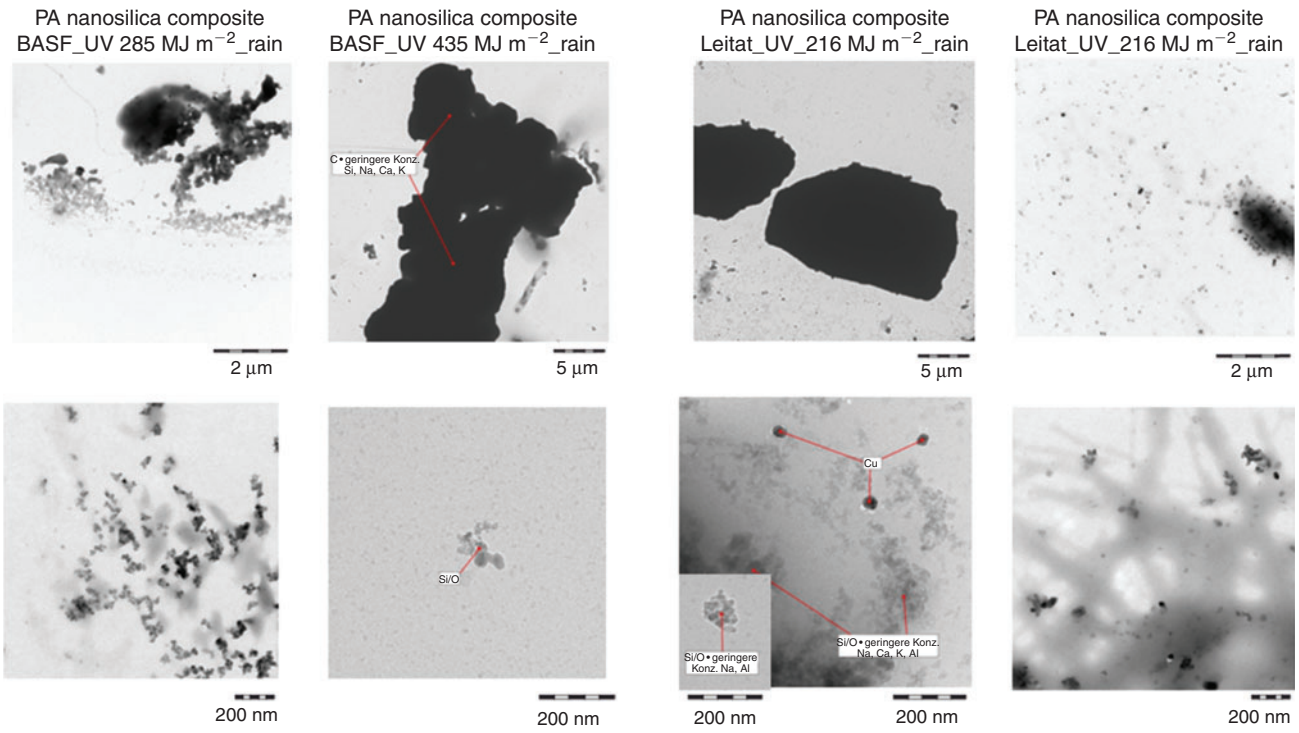

Fig. 10. Transmission electron microscopy (TEM) of induced release fragments from polyamide (PA) nanosilica composite (UV + rain aging at LEITAT or BASF, followed by immersion and sonication release at BASF). A complete reproduction of 102/18 min dry/rain cycle, immersion and detection (first *v.* second column) showed the same polydisperse fragments. A complete reproduction of 1/29 min wet/dry cycle, immersion and detection (third *v.* fourth column) also gave similar results. The different rain cycles at similar UV dose (first *v.* third column) did not result in significantly different fragments, with both polymer–nanosilica structures and some isolated nanosilica clusters released after both protocols.

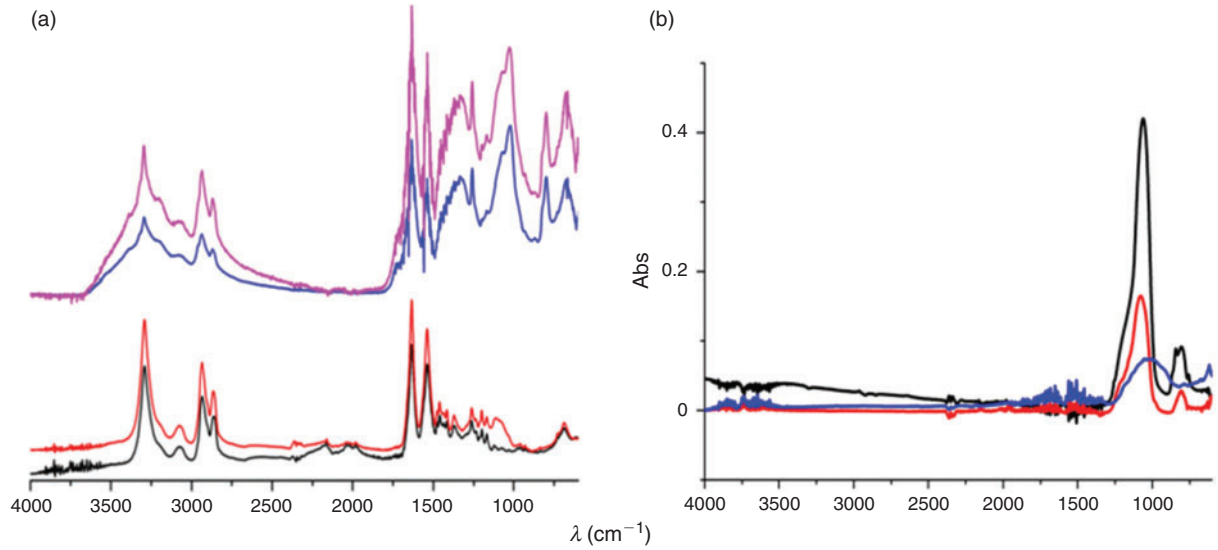

Fig. 11. (a) Fourier-transform infrared (FTIR) spectra of recovered fragments from run-off waters during UV + rain weathering: blue, fragments of neat polyamide (PA); pink, fragments of PA nanosilica composite. The as-produced samples serve as benchmark (lower spectra), black, neat PA; red, PA nanosilica composite. (b) FTIR spectra after calcination: blue, fragments of PA nanosilica composite released after aging; red, PA nanosilica composite; black, nanosilica.

showed the presence of a small amount of silicon, although nanosilica particles were not identifiable in the region analysed. These results are consistent with those obtained by FTIR and TGA analyses, indicating clearly an external or synthetic silicon contamination in the neat PA sample (see Fig. S3 and Table S1).

EDX analysis of release fragments from the nanocomposite revealed the characteristic elemental composition of silica nanoparticles (Fig. 8). The sharp contrast of nanosilica seen in TEM images (Figs 10, S11) and the pronounced bright particulates in the dark field TEM (Fig. S11) also suggested that nanosilica was in the released fragments from the nanocomposite, but not from the neat PA.

Release fragments recovered from the run-off waters of UV + rain aging of the PA–nanosilica composite were analogously analysed by FTIR and TGA techniques, and the results were compared to non-aged data in order to identify the composition of the fragments. For both neat PA and PA nanosilica composite, the FTIR spectra (Figs 11a, S12a) of released fragments exhibited the same absorption bands that can be attributed to the vibrations of the degraded PA matrix. The same conclusions can be drawn from the more sensitive transmission FTIR measurement of the release fragments in KBr discs (Fig. S12b). Comparing the four samples (starting material and recovered fragments), the shape of the bands at ~3400 and ~1600 cm^{-1}, which correspond to amide groups, have broadened considerably after aging. This reflects the chemical degradation of the PA matrix with the formation of a variety of compounds containing OH and C=O groups, such as peroxides, carboxylic acids and their hydrogen bonding among themselves or with other polar groups, such as NH. These results are in good agreement with chemical changes of the polymer matrix (Fig. 4) where the degradation was also noticeable, e.g. a loss of amide bonds (decreased intensity of the bands 3280, 1640 and 1538 cm^{-1}) and gain of carboxylic acids (1708 cm^{-1}) and imide groups (1688 cm^{-1}). There was also a presence of the bands associated with nanosilica or siloxanes in the spectrum of the release fragments, e.g. the bands at 799, 1069 and 1259 cm^{-1}, respectively attributed to Si–O bending, Si–O–Si stretching, and Si–C stretching, indicating the release of nanosilica from the nanocomposite during aging. Calcination at 700 °C for 30 min should effectively remove all polymer substances in the release fragments. This would help to provide information about the remaining inorganic material (nanosilica) in the recovered samples. To effectively observe the characteristic bands corresponding to nanosilica and siloxanes hidden under the bands of the degraded matrix, FTIR was repeated after calcination of the original nanosilica, of a non-aged PA–nanosilica composite and release fragments from the polymer–nanocomposite during aging. The results are displayed in Fig. 11b. Except for some broadening, FTIR spectra of these three calcinated samples overlapped, confirming that the recovered fragments of the PA–nanosilica composite contained nanosilica. As a cross-check, the calcinated samples were also imaged by TEM (Fig. S13).

From the results presented above and in the Supplementary material, it is clear that FTIR (Fig. 11) and TGA (Fig. S14, Table S2) techniques were both not capable of providing the quantity of nanosilica in the release fragments. We, therefore, performed an inductively coupled plasma–mass spectrometry (ICP-MS) analysis of the release fragments. Although ICP-MS cannot distinguish Si from siloxanes, Si-based contaminations or intentionally embedded nanosilica, it has been proven previously as a sensitive technique to quantify nanosilica released or accumulated on the surface of a polymer nanocomposite.[17,19,20,29] Accordingly, a sample of immersion water from a PA–nanosilica composite exposed in the NIST SPHERE at 833 MJ m^{-2} was analysed by ICP-MS. It recorded an Si amount of 0.060 mg mL^{-1}, which represents only a 5 % fraction of the total released mass of 1.22 mg mL^{-1} (AUC), or a 10 % fraction if assuming Si bound as SiO_2. However, the total released mass should contain only 0.023 mg mL^{-1} of Si, if the released fragments had the same composition as the bulk PA–nanosilica composite.

Discussion of release phenomena observed specifically for polyamide nanosilica composites

The accumulation of silica nanoparticles on the PA–nanocomposite surface with UV irradiation is due to the removal of the PA matrix by photodegradation, similar to that observed for silica nanoparticles and MWCNTs on epoxy nanocomposite surfaces.[5,9,11,28,29,31,32] The measured mass loss of the specimen of 2.5 % at 833 MJ m^{-2}, corresponds to 3×10^6 mg m^{-2}, whereas the maximum release by immersion and ultrasonication is 8×10^3 mg m^{-2}. The large gap in the mass balance highlights the prevalence of polymer degradation and removal over nanofiller migration as the origin of accumulation.

After UV aging of a previous batch of the same PA nanosilica composite, we reported that nanosilica was detected only subsurface by SEM, EDX and XPS.[10] However, the SEM image in Fig. S7 and XPS results in Fig. 5 show that the UV dose used previously was just at the threshold (100 MJ m^{-2}) of where nanosilica clearly emerges on the surface. The presence of silica nanoparticles on the PA–nanosilica composite surface as revealed now by AFM and SEM in Fig. 2 is similar to those shown for epoxy–nanosilica composites irradiated with the same UV light source at intermediate and high doses.[29] Fig. 1 provides no evidence of preferential nanosilica release under dry conditions from the nanocomposite after 833 MJ m^{-2} of UV radiation. Nguyen et al.[29] also observed the mass loss of both neat epoxy and epoxy–nanosilica composites was mostly linear with UV irradiation dose, but they reported that the rate of mass loss of the epoxy–nanosilica composite was substantially greater than that of the neat epoxy. Furthermore, they also detected a dry release of silica nanoparticles after 700 MJ m^{-2} UV irradiation. The mass loss result of the PA nanocomposite is also different from that of an epoxy–MWCNT composite, in which the mass loss of the CNT composite was found to be less than that of the neat epoxy.[5] This was attributed to the ability of MWCNTs to photostabilise the epoxy polymer.

The differences observed in surface cracking characteristics are related to material mechanical property. The difference in crack width between the neat and nanocomposite PA indicates a marked difference in the stress strain behaviour between these two materials. As seen in the AFM results, and confirmed by the SEM image at the highest dose, a substantial amount of silica nanoparticles had accumulated on the surface of the PA–nanosilica composite as a result of UV irradiation. Therefore, changes in crack properties (e.g. density, size, length) with UV irradiation will likely affect both the amounts of silica nanoparticles accumulated on the nanocomposite surface and released to the environment. A quantitative study is needed to determine the effects of UV-induced cracking on the amount of silica nanoparticles accumulated on the PA nanocomposite surface. LSCM in combination with image analysis is a good technique for quantifying the crack density, and AFM and especially SEM with backscatter detection are viable techniques for following the accumulation of nanoparticles on the nanocomposite surface.

Spontaneous release of SiO_2 from paints into run-off water was investigated by the NanoHouse project, and confirmed that the majority of the particulate Si was contained in composites, representing the paint matrix, whereas only few single SiO_2 nanofillers were detected.[7] Additional leaching experiments addressed the ratio between Si ions and particulate SiO_2,[33] whereas our investigations focus on the particulate fractions and obtain excellent accord on the release characteristics.

Spontaneous release from plastics into run-off water was investigated by the NanoPolyTox project, and first results on the degradation of the bulk material[31] and of the released fragments in run-off water[17] were reported. The tests in the same setup (Suntest XXL+) followed the same protocol of 1/29 min wet/dry, and the run-off waters were collected in the same way as in the present study. By comparison of 18 nanocomposites (nanofillers MWCNT, nanoclays, SiO_2, TiO_2, ZnO, compounded in matrices PA, polyproylene (PP), ethylene vinyl acetate (EVA)), the compatibility between nanofiller and matrix, as expressed by a homogeneous nanofiller dispersion in the composite, emerged as the main determinant of a low probability of release during weathering. Substantial aggregation of nanofillers in the matrix such as propyl-functionalised nanosilica in polypropylene led to an over-representative accumulation of nanosilica in the run-off waters.[17] Following these rules, the PA–nanosilica composite of the present study would be regarded as partially agglomerated, but we find that the over-representation of nanosilica in the released fragments is limited.

However, quantitation suffers from the composite nature of the released fragments, and possibly from uncontrolled sources of Si. Despite a clear identification of nanosilica in the release fragments, as evidenced by various analyses, the fragments recovered from the run-off waters were dominated by the organic material that resulted in practically the same amounts of release fragments from both neat PA and PA–nanosilica composites. The presence, albeit a low level, of inorganic impurities in the neat PA (Table S2) is not sufficient to explain this experimental observation. The result suggests that another Si source during the weathering process has probably contributed to the amount of silica in the release fragments.

In a combined interpretation of the results on released fragments from ICP-MS, TEM, AUC, gravimetry, FTIR and TGA, we found that the released fragments are ~10 % nanosilica and 90 % polymer, thus dominated by polymer, but enriched in SiO_2 compared to the as-produced composite. This is consistent with the analysis of the bulk surface by SEM, EDX, AFM, FTIR and XPS, indicating the accumulation of the UV-persistent nanofiller on the surface as the polymer degrades.

A comparison of fragment mass in run-off water from rain cycles (LEITAT/NanoPolyTox protocol, see red cross in Fig. 6) and induced release (on the same sample after weathering, see Fig. 7) shows that 98 % of the total released fragments are in the run-off water and only 2 % require ultrasonication to release. The comparison between different rain cycles, between spontaneous release (1000 h) and immersion (24 h), and between zero shear and ultrasonication during immersion all point to a low threshold of mechanical energy required for the release of nanoparticles from degraded polymers (Table 3).

In contrast, Hirth and co-workers investigated the release probability of nanotubes (MWCNTs) from a thermoplastic polyurethane matrix by using the same UV + immersion protocol as in the present study.[18] They observed a release increase of at least 300 % between shaker treatment and ultrasonication in contrast to a factor of ~50 % determined here for PA–nanosilica composites. This suppression of spontaneous release was attributed to the strong van der Waals forces of the collapsed and entangled MWCNT network remaining on the surface. Furthermore, the mass loss of epoxy with embedded MWCNTs was significantly reduced compared to the mass loss of neat epoxy, attributed to the black colour and UV-protective effects of MWCNTs.[5,12]

We conclude that silica nanoparticles, unlike MWCNTs, are spontaneously released from degraded polymer matrices: Polymer hydrolysis, degradation, scission and evaporation dominates by far over nanoparticle migration, and results in enrichment of nanosilica in the remaining surface layer, from where it can be released with no external forces other than the presence of water.[4] Furthermore, nanosilica neither protects nor promotes the PA degradation, and PA produces a variety of release fragments from 10 nm to several micrometres in diameter during UV aging of nanocomposites.

Assuming that structural parts with typical dimensions of ~5-mm thickness degrade under UV light, our measured total release of ~10 g m^{-2} throughout a simulated 10-year use phase corresponds to 0.01 % of the part's mass. In these fragments, the released nanosilica accounted for up to 0.001 % of the part's mass, determined by the organic/inorganic ratio of the total release, but only 10 % thereof are released as free or clustered nanosilica (not bound to organics), based on the above estimates. These release rates may decrease further for commercial products optimised for outdoor applications with the addition of UV stabilisers – unlike the unstabilised polymer tested here. For environmental mass flow estimates, the use phase is hence a relatively small source compared to production, recycling and disposal phases.

Conclusion on aging and release protocols

Several degradation protocols to simulate outdoor aging and several methods to identify, quantify and characterise the remaining bulk material and the released fragments were compared and combined for a polyamide with 4 % nanosilica composite. We found that aging conditions are very critical, whereas the sampling protocol tolerates some differences. Analysis methods that were most helpful to assess the release phenomena are incorporated into the finally recommended protocol.

By the comparison of two different UV radiation sources, the degradation and release phenomena were qualitatively very similar, but the progression of polymer matrix degradation and the ensuing release rates differed considerably (Table 3). It should be noted that the UV source of the 140 W m^{-2} intensity is a mercury lamp and that of the 60 W m^{-2} is a xenon arc. In addition to the intensity difference given above, the spectroscopic distributions of these two UV lamps are markedly different. And finally, the sample holder in the NIST SPHERE maintained a temperature of 65 °C, whereas the Suntest XLS+ maintains a *blackbody* temperature of 65 °C by the ventilation of the entire chamber (Table 1). It is reasonable to assume that the white PA polymers maintain in the Suntest XLS+ a temperature that is closer to room temperature than in the NIST SPHERE sample holder, and this parameter could actually be the main cause of the differing release rates.

Although the results of this study show that the degradation mechanism imposed by the mercury lamp is similar to that of the xenon arc or outdoor exposures, standardised testing protocols for release of nanomaterials from polymer nanocomposites should rely on already standardised irradiation equipment or be exposed additionally to different outdoor locations. This is particularly important for polymer matrices such as PAs, polyesters and acrylic melamines, which are sensitive to both UV radiation and water.[12] For such polymers, the total degradation in a UV moist environment is often not the sum of photodegradation and hydrolysis. This is because photo-oxidation products, such as carboxylic acids, tend to autocatalyse and accelerate the hydrolysis reactions, whereas carbonyl compounds generated by hydrolytic degradation can absorb UV radiation and initiate the photo-oxidation process.[5,12,18,19]

Regarding sampling and release protocols, the analysis of spontaneous release in run-off waters is currently the most direct simulation of real-world outdoor aging. The soon-to-be-published NanoPolyTox results will offer a benchmark for release effects. On the downside, the ISO 4892 conditions[22] cannot be used directly, but rain cycles are reduced by a factor of 9 to reduce the workload for freeze-drying of run-off water, spraying equipment is required, and parallelisation of comparative testing is limited to avoid mixing of run-offs. Some of these disadvantages may not be severe, because we found that the modification of rain cycles had little effect (Table 3), and spraying equipment is fairly inexpensive: Despite the strong additional effects by hydrolysis – which speeds up degradation and leads to a 20-fold more release (Table 3) – TEM finds that the characteristics of fragments from spontaneous or induced release by aging of a PA–nanosilica composite were qualitatively undistinguishable (Table 3).

The alternative immersion protocol offers the advantage that synergy of degradation and mechanical stress is simulated. For decentralised laboratories, ISO-conformed dry UV irradiation followed by immersion in water should be easy to accomplish. For research laboratories, multipurpose UV + rain weathering equipment with hundreds of samples in parallel can be employed to include the hydrolysis effects, followed by the immersion for release characterisation. On the downside, only the release characteristics were identical to the spontaneous run-off waters in the present study, not the release quantity. Similar ranges of release (up to 56 mg m^{-2} Si or 1123 mg m^{-2} of epoxy–SiO_2 fragments) are obtained by another variant of induced release, namely spraying water onto vertically held large (71.2 cm^2) samples for 10 min between or after irradiations and measuring the Si content in the run-off by inductively coupled plasma–optical emission spectroscopy (ICP-OES).[20] A closely related immersion approach was developed at CEREGE Centre Européen de Recherche et d'Enseignement des Géosciences de l'Environnement). They irradiated by 105 W cm^{-2} dry (300–400 nm) and immersed specimen for 1.5 h four times per week without shear forces, analysed by ICP-MS, and successfully benchmarked results to an adapted UV + rain protocol (Suntest XLS+, 65 W m^{-2}, rain four times per week).[19] In our study, the immersion protocol tolerated variations of its parameters without critical changes of the release characteristics or rate (Table 3), and should hence also be easily transferrable between laboratories. We propose the following protocol for study of material release by aging of polymer nanocomposites. Depending on equipment availability, some steps may be omitted:

1. Prepare specimens having at least 30-cm^2 irradiation area.
2. Perform weathering by UV dry and (optionally) UV + rain, measure mass loss at least up to 3000 h under ISO4892-2 conditions (435 MJ m^{-2}).
   a. Optionally: cut 1 cm^2 and analyse bulk degradation by SEM, FTIR and XPS.
3. Immerse weathered specimens in a minimal volume of water (below 5 mL)
   a. analyse the immersion water by ICP-MS to quantify the total release. Scale the obtained release by the ratio between the mass loss from dry and wet weathering to account for hydrolysis of the matrix.

   b. analyse by TEM to identify the released fragments. Optionally supported by EDX or calcination and repeated TEM.
   c. Optionally: deagglomerate the released fragments and centrifuge (or filter), analyse the supernatant (or filtrate) by ICP-MS to quantify *free* nanofiller.
   d. Optionally: deagglomerate the released fragments (see *Methods*) and perform FFF or AUC to quantify the size distribution of fragments and therein the content of free nanofiller.
4. Optionally: repeat the immersion with gradually increasing shear to characterise the release probability under different use scenarios.
5. Caveats:
   a. Ensure a homogeneous distribution of nanofiller up to the sample surface, and completely remove surface layers from sample preparation
   b. Use positive and negative controls for the detection of nanofiller in immersion water.
   c. Do not rely on TGA or FTIR for the identification of fragment composition.

For nanofillers that do not contain metal elements, ICP-MS needs to be replaced with an alternative technique, but these (e.g. UV-Vis, Raman)may not have the capability to quantify a low concentration of released nanoparticles. One possibility is analysis of the catalyst in or on CNTs for tracing CNT release, and is thus an important topic for future studies.[12,32]

With the above protocol, simplified UV (rain) + immersion protocols can at least partially replace, complement and extend dedicated weathering apparatus with run-off collection. Because neat polymers release substantial fragments with nanometre and micrometre dimensions after aging, comparative testing between the neat polymer and the nanocomposite and chemical identification of fragments is advised. Our results lay the ground for a full interlaboratory validation, because we found that the characteristics of release fragments – which are the essential input for fate, transport and (eco-)toxicological testing – were not critically dependent on the remaining differences of the protocols that were employed here: The released fragments were always a polydisperse mixture of predominantly composite fragments from the nanoscale up to several micrometres in diameter, and of clustered or free nanosilica. The fraction of free nanofiller was identified by microscopy, but could not be quantified. To achieve reproducible, standardised release rates, highly controlled aging conditions are most critical.

Supplementary material

Supporting online material is available at http://www.publish.csiro.au/?act=view_file&file_id=EN14072_AC.pdf and includes characterisation of materials before aging by FTIR, TGA, TEM, characterisation of bulk material after aging by FTIR, XPS, SEM, AFM and characterisation of released fragments by AUC, TEM, FTIR, calcined-TEM, TGA.

Author contributions

S. Vazquez-Campos, T. Nguyen and W. Wohlleben designed the study and co-wrote the manuscript; W. Wohlleben initiated the cooperation, supervised and analysed the weathering, immersion and colloidal characterisation of fragments, and finalised the manuscript; T. Nguyen analysed and interpreted mass loss, AFM and FTIR data; G. Vilar, D. González-Gálvez and E. Fernández-Rosas performed accelerated aging and collected released nanomaterials from run-off waters and characterised released nanomaterials by TGA, FT-IR and TEM-EDX; G. Vilar co-wrote the manuscript and D. González-Gálvez participated in the final manuscript correction and prepared the figures; C. Gabriel synthesised the nanocomposite material; S. Hirth measured and analysed XPS results of sample degradation; T. Frechen characterised weathered surfaces and released fragments by electron microscopy; D. Stanley performed weathering at NIST and measured mass loss and chemical degradation as a function of UV exposure; J. Gorham measured and analysed XPS results of sample degradation and wrote the XPS portion; L. Sung supervised the weathering experiment and AFM and confocal microscopy measurements; H.-C. Hsueh measured AFM images; Y.-F. Chuang measured confocal microscopy images and surface roughness with UV exposures.

Acknowledgements

This work was partially supported by BMBF project nanoGEM (Förderkennzeichen 03X0105B). We gratefully acknowledge the excellent laboratory support by Klaus Vilsmeier and editorial support by Maël Boland.

References

[1] B. Nowack, B. Ranville, S. Diamond, J. A. Galego-Urrea, C. Metcalfe, J. Rose, N. Horne, A. A. Koelmans, S. J. Klaine, Potential scenarios for nanomaterial release and subsequent alteration in the environment. *Environ. Toxicol. Chem.* **2012**, *31*, 50. doi:10.1002/ETC.726

[2] M. R. Wiesner, G. V. Lowry, K. L. Jones, M. F. Hochella Jr, R. T. di Giulio, E. Casman, E. S. Bernhardt, Decreasing uncertainties in assessing environmental exposure, risk, and ecological implications of nanomaterials. *Environ. Sci. Technol.* **2009**, *43*, 6458. doi:10.1021/ES803621K

[3] E. J. Petersen, L. Zhang, N. Mattison, D. O'Carroll, A. Whelton, N. Uddin, T. Nguyen, Q. Huang, T. Henry, R. Holbrook, K. Chen, Potential release pathways, environmental fate, and ecological risks of carbon nanotubes. *Environ. Sci. Technol.* **2011**, *45*, 9837. doi:10.1021/ES201579Y

[4] T. Nguyen, W. Wohlleben, L. Sung, Mechanisms of aging and release from weathered nanocomposites, in *Safety of Nanomaterial along their Lifecycle: Release, Exposure and Human Hazards* (Eds W. Wohlleben, T. Kuhlbusch, C. M. Lehr, J. Schnekenburger) **2014**, Ch. 14, pp. 315–334 (Taylor & Francis: boca Raton, FL).

[5] T. Nguyen, B. Pellegrin, C. Bernard, X. Gu, J. M. Gorham, P. Stutzman, D. Stanley, A. Shapiro, E. Byrd, R. Hettenhouser, J. Chin, Fate of nanoparticles during life cycle of polymer nanocomposites. *J. Phys. Conf. Ser.* **2011**, *304*, 012060. doi:10.1088/1742-6596/304/1/012060

[6] J. P. Kaiser, M. Roesslein, L. Diener, P. Wick, Human health risk of ingested nanoparticles that are added as multifunctional agents to paints: an *in vitro* study. *PLoS ONE* **2013**, *8*, e83215. doi:10.1371/JOURNAL.PONE.0083215

[7] A. Al-Kattan, A. Wichser, R. Vonbank, S. Brunner, A. Ulrich, S. Zuin, Y. Arroyo, L. Golanski, B. Nowack, Characterization of materials released into water from paint containing nano-SiO_2. *Chemosphere*, in press. doi:10.1016/J.CHEMOSPHERE.2014.02.005

[8] B. Nowack, R. M. David, H. Fissan, H. Morris, J. A. Shatkin, M. Stintz, R. Zepp, D. Brouwer, Potential release scenarios for carbon nanotubes used in composites. *Environ. Int.* **2013**, *59*, 1. doi:10.1016/J.ENVINT.2013.04.003

[9] E. J. Petersen, T. Lam, J. M. Gorham, K. C. Scott, C. J. Long, D. Stanley, R. Sharma, J. Alexander Liddle, B. Pellegrin, T. Nguyen, Methods to assess the impact of UV irradiation on the surface chemistry and structure of multiwall carbon nanotube epoxy nanocomposites. *Carbon* **2014**, *69*, 194. doi:10.1016/J.CARBON.2013.12.016

[10] W. Wohlleben, S. Brill, M. W. Meier, M. Mertler, G. Cox, S. Hirth, B. von Vacano, V. Strauss, S. Treumann, K. Wiench, L. Ma-Hock, R. Landsiedel, On the lifecycle of nanocomposites: comparing released fragments and their vivo hazard from three release mechanisms and four nanocomposites. *Small* **2011**, *7*, 2384. doi:10.1002/SMLL.201002054

[11] W. Wohlleben, M. W. Meier, S. Vogel, R. Landsiedel, G. Cox, S. Hirth, Z. Tomovic, Elastic CNT-polyurethane nanocomposite: synthesis, performance and assessment of fragments released during use. *Nanoscale* **2013**, *5*, 369. [Published online 21 November 2012]. doi:10.1039/C2NR32711B

[12] C. Kingston, R. Zepp, A. Andrady, D. Boverhof, R. Fehir, D. Hawkins, J. Roberts, P. Sayre, B. Shelton, Y. Sultan, V. Vejins, W. Wohlleben, Release characteristics of selected carbon nanotube polymer composites. *Carbon* **2014**, *68*, 33. [Published online early 26 November 2013]. doi:10.1016/J.CARBON.2013.11.042

[13] C. Bernard, T. Nguyen, B. Pellegrin, R. D. Holbrook, M. Zhao, J. Chin, Fate of graphene in polymer nanocomposite exposed to UV radiation. *J. Phys. Conf. Ser.* **2011**, *304*, 012063. doi:10.1088/1742-6596/304/1/012063

[14] J. Lemaire, J. L. Gardette, A. Rivaton, A. Roger, Dual photochemistries in aliphatic polyamides, bisphenol A polycarbonate and aromatic polyurethanes – a short review. *Polym. Degrad. Stabil.* **1986**, *15*, 1. doi:10.1016/0141-3910(86)90002-9

[15] J. F. Rabek, *Polymer Photodegradation: Mechanisms And Experimental Methods* **1995**, pp. 296–306 (Springer: New York).

[16] A. Roger, D. Sallet, J. Lemaire, Photochemistry of aliphatic polyamides. 4. Mechanisms of photooxidation of polyamides 6, 11, and 12 at long wavelengths. *Macromol.* **1986**, *19*, 579. doi:10.1021/MA00157A015

[17] M. Busquets-Fité, E. Fernandez, G. Janer, G. Vilar, S. Vazquez-Campos, R. Zanasca, C. Citterio, L. Mercante, V. Puntes, Exploring release and recovery of nanomaterials from commercial polymeric nanocomposites. *J. Phys. Conf. Ser.* **2013**, *429*, 012048. doi:10.1088/1742-6596/429/1/012048

[18] S. Hirth, L. G. Cena, G. Cox, Z. Tomovic, T. M. Peters, W. Wohlleben, Scenarios and methods that induce protruding or released CNTs after degradation of composite materials. *J. Nanopart. Res.* **2013**, *15*, 1504. doi:10.1007/S11051-013-1504-X

[19] L. Scifo, P. Chaurand, A. Masion, M. Auffan, M.-A. Diot, J. Labille, J. Y. Bottero, J. Rose, Release of CeO_2 nanoparticles upon aging of acrylic wood coatings. Presented at NanoSafe2012, 15 November 2012, Grenoble, **2012**. Available at http://www.nanosafe.org/scripts/home/publigen/content/templates/show.asp?P=143&L=EN&ITEMID=57 [Verified 15 July 2014].

[20] T. Nguyen, Quantitative studies of photo-induced surface accumulation and release of nanoparticles in polymer nanocomposites. Presented at NanoSafe2012, 15 November 2012, Grenoble, **2012**. Available at http://www.nanosafe.org/scripts/home/publigen/content/templates/show.asp?P=143&L=EN&ITEMID=57 [Verified 15 July 2014].

[21] D. Göhler, A. Nogowski, P. Fiala, M. Stintz, Nanoparticle release from nanocomposites due to mechanical treatment at two stages of the life-cycle. *J. Phys. Conf. Ser.* **2013**, *429*, 012045. doi:10.1088/1742-6596/429/1/012045

[22] *ISO 4892–2: Plastics — Methods of Exposure to Laboratory Light Sources. Part 2: Xenon-Arc Lamps* **2006**. [Updated 2013].

[23] J. Chin, E. Byrd, N. Embree, J. Garver, B. Dickens, T. Finn, J. Martin, Accelerated UV weathering device based on integrating sphere technology. *Rev. Sci. Instrum.* **2004**, *75*, 4951. doi:10.1063/1.1808916

[24] W. Wohlleben, Validity range of centrifuges for the regulation of nanomaterials: from classification to as-tested coronas. *J. Nanopart. Res.* **2012**, *14*, 1300. doi:10.1007/S11051-012-1300-Z

[25] R. P. Carney, J. Y. Kim, H. Qian, R. Jin, H. Mehenni, F. Stellacci, O. M. Bakr, Determination of nanoparticle size distribution together with density or molecular weight by 2D analytical ultracentrifugation. *Nature Commun.* **2011**, *2*, 335. doi:10.1038/NCOMMS1338

[26] P. N. Thanki, R. P. Singh, Progress in the area of degradation and stabilization of nylon 66. *J. Macromol. Sci: Polym. Rev.* **1998**, *38*, 595. doi:10.1080/15583729808546033

[27] D. J. Skrovanek, S. E. Howe, P. C. Painter, M. M. Coleman, Hydrogen bonding in polymers: infrared temperature studies of an amorphous polyamide. *Macromol.* **1985**, *18*, 1676. doi:10.1021/MA00151A006

[28] N. B. Colthup, L. H. Daly, S. E. Wiberley, *Introduction To Infrared And Raman Spectroscopy* **1990** (Academic Press: San Diego, CA).

[29] T. Nguyen, B. Pellegrin, C. Bernard, P. Stutzman, J. M. Gorham, X. Gu, L. L. Yu, J. W. Chin, Characterization of surface accumulation and release of nanosilica during irradiation of polymer nanocomposites. *J. Nanosci. Nanotechnol.* **2012**, *12*, 6202. doi:10.1166/JNN.2012.6442

[30] J. M. Gorham, T. Nguyen, C. Bernard, D. Stanley, R. D. Holbrook, Photo-induced surface transformations of silica nanocomposites. *Surf. Interface Anal.* **2012**, *44*, 1572. doi:10.1002/SIA.5075

[31] G. Vilar, E. Fernandez-Rosas, V. Puntes, V. Jamier, L. Aubouy, S. Vazquez-Campos, Monitoring migration and transformation of nanomaterials in polymeric composites during accelerated aging. *J. Phys. Conf. Ser.* **2013**, *429*, 012044. doi:10.1088/1742-6596/429/1/012044

[32] S. Froggett, S. Clancy, D. Boverhof, R. Canady, A review and perspective of existing research on the release of nanomaterials from solid nanocomposites. *Part. Fibre Toxicol.* **2014**, *11*, 17. doi:10.1186/1743-8977-11-17

[33] S. Zuin, A. Massari, A. Ferrari, L. Golanski, Formulation effects on the release of silica dioxide nanoparticles from paint debris to water. *Sci. Total Environ.* **2014**, *476–477*, 298. doi:10.1016/J.SCITOTENV.2014.01.029